*Manuscript
Click here to view linked References

# Optical and Photoconductive Properties of Indium Sulfide Fluoride Thin Films

Y. Vygranenko[1*], M. Vieira[1,2], G. Lavareda[1,3], C. Nunes de Carvalho[3,4], P. Brogueira[4,5], A. Amaral[4,5], N. P. Barradas[6], E. Alves[7]

[1]CTS-UNINOVA, Quinta da Torre, 2829-516 Caparica, Portugal

[2]Departamento de Engenharia Electrónica e Telecomunicações e de Computadores, ISEL, Lisboa, Portugal

[3]Departamento de Ciência dos Materiais, Faculdade de Ciências e Tecnologia, Universidade Nova de Lisboa, Portugal

[4]CeFEMA and [5]Departamento de Física, Instituto Superior Técnico, Universidade de Lisboa, Portugal

[6] Centro de Ciências Tecnológicas e Nucleares, Lisboa, Portugal

[7]Instituto de Plasmas e Fusão Nuclear, Lisboa, Portugal

This work reports on transparent semiconducting indium sulfide fluoride (ISF) thin-films exhibiting high sensitivity to ultraviolet radiation. The films were deposited on fused silica and silicon substrates using a radio-frequency plasma-enhanced reactive thermal evaporation system. The deposition was performed evaporating pure indium in $SF_6$ plasma at a substrate temperature of 423 K. Rutherford backscattering measurements were used to determine the chemical composition of the films deposited on silicon substrates. The surface morphology was studied using scanning electron microscopy technique. The film characterization includes electrical, optical, and photoconductivity measurements. The synthesized compound is highly-resistive (~700 MΩ-cm at 300 K) and exhibits an evident semiconducting behavior. The activation energy of 0.88 eV is deduced from the temperature dependence of electrical resistivity. The indirect band energy gap of 2.8 eV is determined from transmittance spectra of the ISF films. The photoconductivity band is centered at 345 nm wavelength. The photoconductivity spectrum also shows the Urbach tail with a characteristic energy of 166 meV. ISF is a promising candidate for a buffer layer in chalcogenide-based solar cells.

**Keywords**: indium sulfide fluoride, thin-films, amorphous semiconductors, optical properties, photoconductivity, photovoltaics

## 1. Introduction

Chalcogenide-based solar cells exhibit the highest energy conversion efficiencies among the thin film photovoltaic devices. Recently, the $Cu(In,Ga)Se_2$/CdS heterojunction solar cell with record efficiency of 22.6% was reported [1]. Further progress in chalcogenide photovoltaics is in low-cost, Cd-free technology. To avoid toxic heavy-metal-containing waste in the PV module production and utilization, the substitution of CdS by alternative materials is one of the technological challenges. Various relevant materials such as Zn(O,S, Se), $Zn_{1-x}Mg_xO$ and indium sulfide derivatives have been investigated and used in fabrication of chalcogenide-based solar cells [2]. Among them indium sulfide ($In_2S_3$) is most attractive because of its stability, wide bandgap, and photoconductive behavior. $In_2S_3$ thin films have been synthesized by numerous deposition techniques [3]. However, each technique provides specific crystalline, electrical and optical properties, which are crucial for the solar cell performance [4]. Until now, atomic layer deposition and ionic layer gas atomic reaction techniques have been the two most successful for $In_2S_3$ buffer layers, yielding maximum energy conversion efficiencies up to 16.4% and 16.1%, respectively [5,6]. The $In_2S_3$-buffered cells typically show lower $V_{oc}$ in comparison to CdS-buffered devices that is attributed to recombination via states associated with a lattice mismatch at the heterojunction interface. In addition, the buffer/window interface recombination component may also be significant [2]. Furthermore, diffusion of Cu and Na from the absorber to the buffer layer, dependent upon deposition temperature and annealing temperature, can worsen the electronic properties of $In_2S_3$ [2]. Perhaps incorporation of amorphous derivatives of indium sulfide instead of micro-crystalline $In_2S_3$ would help to solve the mentioned technological issues. Using the amorphous buffer, it is easier to form heterojunction with low density of interfacial defects similar to that in the heterojunction with an intrinsic thin layer solar cells [7]. The path between the grains for contaminant diffusion could be also eliminated. Another advantage is that amorphous materials can be deposited uniformly over a large area, what makes them suitable for the large-scale fabrication.

In this paper, we report on indium sulfide fluoride (ISF) thin-films deposited by plasma-enhanced reactive thermal evaporation (rf-PERTE). The study of film composition, structure, and surface morphology is a starting point of this work. Then, we present and discuss the electrical and optical properties of this material. Furthermore, special attention is given to the photoconductive properties of ISF films.

## 2. Experimental

The films for this study were prepared using an automated rf-PERTE system, which is based on a bell jar type vacuum chamber with a pumping group including diffusion and mechanical pumps. The distance between the tungsten boat and the sample holder is 32 cm. For plasma assisting, an rf-electrode in the form of a copper ring is placed in the half-way between them. The shutter is mounted in a distance of about 15 mm from the sample holder surface to prevent the exposure of the samples to plasma before the deposition. Injection of reactive gas into chamber is controlled by a SmartTrak 100 Series mass flow controller. A Genesys$^{TM}$ series programmable regulated power supply and a Cesar$^{TM}$ Generator, Model 136, are used as dc and rf power sources, respectively. The ISF films were deposited on fused silica and crystalline Si substrates by evaporating pure indium in $SF_6$ plasma at a substrate temperature ranging from 313 to 423 K. The deposition conditions were $4 \cdot 10^{-2}$ Pa pressure, 15 sccm gas flow, 35 W rf-power, and a deposition rate of about 0.5 nm/s. The film thickness was determined by a Veeco Dektak III. It was in the range of 240 – 300 nm due to deposition non-uniformity within an area of 10×10 cm. The best films in terms of photoconductive properties were obtained at 423 K. These films were subjected to full characterization reported below.

Rutherford backscattering (RBS) analysis was used to determine the chemical composition of films on Si substrates as well as depth distributions. RBS measurements were made in a small chamber with three detectors: a standard at 140º, and two pin-diode detectors located symmetrically to each other, both at 165º. Detectors under 165 degrees were used to measure the scattered ions coming from the sample. Spectra were collected for 2 MeV $^4He^+$ ions at normal incidence.

Grazing-incidence X-ray diffraction (XRD) measurements are performed using a D8 ADVANCE diffractometer with DAVINCI.DESIGN and a LINXEYE-XE detector (Cu Kα$^o$λ=1.54Å) in the grazing incidence geometry, with an incident beam angle of 1.5°.

The film morphology was studied using a Zeiss AURIGA Compact SEM. Samples for electrical characterization were prepared by evaporating Al through a shadow mask to form coplanar contacts. The measurements were performed in a vacuum chamber at about 70 Pa base pressure. The conductivity versus temperature was measured using a Keithley 617 electrometer, and a Keithley 228 A power supply for sensing and temperature control, respectively. The transmittance in the visible and near violet/infra-red regions (200–1200 nm) was measured using a Shimadzu UV-3100 spectrophotometer, without a bare substrate across

the reference beam. The spectral response measurements were performed using a PC controlled setup based on a Triax-120 grating monochromator, a Stanford Research System SR540 light chopper, and a SR530 DSP lock-in amplifier. The system was calibrated in the spectral range of 320–1100 nm using a Thorlabs FDS1010-CAL detector.

## 3. Results and discussion

Figure 1(a) shows a typical RBS spectrum of the ISF film on the Si substrate. The spectrum clearly shows the individual signals from the scattered particles by the In, S, F and O elements. The possibility to fit the individual contribution of each element for the RBS spectrum allows us to obtain an accurate depth profile of the elements present in the film. The lower height of the front edge of the signal of In, S and F is a clear indication of a lower concentration of these elements in the near surface region. The best fit of the results obtained with the NDF software package [8] confirms an increase of oxygen in the surface region leading to a two layer structure of the film which is shown in Fig. 1(b). The enrichment of oxygen at the surface can be explained by the reaction with the moisture present in the ambient atmosphere, which is likely to happen considering the hygroscopic nature of $InF_3$ [9]. The concentration of the different elements in the deeper layer are 32, 16, 47, and 5 at.% for In, S, F and O, respectively. The accuracy of these values is below 5% which is the uncertainty limit of the RBS technique.

Figure 2 shows a typical scanning electron microscope micrograph of the ISF film on the crystalline Si substrate. The film appears uniform, flat, and dense with a fine grained surface aspect. The ISF films were further characterized for structural properties using X-ray diffraction technique. The XRD patterns of as deposited films onto fused silica and crystalline Si substrates reveal their amorphous structure.

The film resistivity ρ was measured in the temperature range of 277 - 345 K. Figure 3 shows the variation of $log(\rho)$ with inverse of temperature for the ISF thin film. The data perfectly follows the $\rho \sim exp(E_a/kT)$ relation leading to the conclusion that the synthesized material is a semiconductor. The deduced thermal activation energy ($E_a$) is 0.88 eV. The resistivity at 300 K is found to be $7 \cdot 10^8$ Ω·cm. For comparison, the electrical resistivity of pure β-$In_2S_3$ has been found around $5 \cdot 10^7$ Ω·cm [10], while a resistivity of $2 \cdot 10^{12}$ Ω·cm has been reported for $InF_3$ films [9].

Figure 4 shows the transmittance spectrum of the ISF film. The transmittance of the fused silica substrate is also shown as a reference curve. The interference peak maxima and substrate transmittance values are about the same at $\lambda > 500$ nm due to low absorption. Strong absorption is observed in UV range. The extinction coefficient $\alpha$ was deduced from the spectrum using the method proposed in [11].

To obtain information about direct or indirect interband transitions in ISF, the dependence of $(\alpha hv)^{1/m}$ on photon energy $hv$ was plotted for m = 0.5 and 2. As shown in Fig. 5, the dependence is almost linear at m = 2 indicating that the optical transition involved is of indirect type. The band gap of 2.83 ±0.05 eV is determined by fitting the linear part of the curve and calculating the intercept with the energy-axes at $\alpha = 0$. The deduced band gap value is closer to values reported for $In_2S_3$ than to 8.15 eV band gap energy for $InF_3$ [9]. Note that there is still controversy about whether $In_2S_3$ has a direct or indirect band gap. In the study on the optical properties of β-$In_2S_3$ single crystal, the reported indirect and direct bandgap energies are 2.24 and 2.64 eV, respectively [12]. Because of the difficulty in preparing stoichiometric $In_2S_3$ thin films with highly crystalline structure, the reported in the literature values of the direct optical band gap vary in a wide range of 1.9 - 2.8 eV [13-16]. Indeed ISF has a wider band gap due to high fluorine content or/and strong structural disorder. An example of impurity-induced band gap widening is $In_2S_3$ containing Na compound, in which the optical band gap increases linearly from 2.15 to 2.90 eV when sodium content varies from 0 to 12 at.% [17]. The indirect nature of the band gap in $In_xS_y$:Na has been also reported elsewhere [18].

Figure 6 shows a spectral-response of the ISF film in the UV-visible spectral range. Using the optical bandgap energy determined from optical data, the signal is referred to the fundamental and sub-bandgap absorption. The photoresponse reaches maximum value at 345 nm wavelength. At longer wavelengths, it decreases exponentially over 3 orders of magnitude within sub-bandgap energy range that can be attributed to optical transitions involving the band tail states. The deduced Urbach energy is 166 meV. This result is an additional confirmation about high structural disorder in ISF compound.

## 4. Conclusion

ISF compound has been synthesized at a low process temperature using the rf-PERTE method. The chemical composition was determined by RBS technique. The semiconducting behavior of the ISF thin film was verified by the dark electrical resistivity measurement

performed in the temperature range of 277 - 345 K. The deduced thermal activation energy is 0.88 eV, and the resistivity is $7 \cdot 10^8$ Ω·cm at 300 K. The absorption coefficient, which was deduced from a transmittance spectrum of the ISF film, was used to evaluate the nature of the band gap and its value. The obtained indirect optical bandgap energy is 2.8 eV that is comparable to a value of 2.9 eV for $In_xS_y$:Na at high (~12 at.%) sodium concentration. The ISF films are highly photosensitive in the ultraviolet A spectral range. The photoconductivity measurements revealed the presence of inter-gap states. Urbach energy of 166 meV was obtained analyzing the spectral response at $hv < E_g$. The presented results support the conclusion that ISF is a wide-gap semiconductor material suitable for photovoltaic and UV-sensing applications.

**Acknowledgements**

The authors are grateful to the Portuguese Foundation of Science and Technology through fellowship SFRH/BPD/102217/2014 for financial support of this research.

**References**

1. P. Jackson, R.Wuerz, D. Hariskos, E. Lotter, W.Witte, M. Powalla, Effects of heavy alkali elements in Cu(In,Ga)Se2 solar cells with efficiencies up to 22.6%, Phys. Status Solidi RRL 10, 8 (2016) 583–586.
2. M. A. Mughal, R. Engelken, R. Sharma, Progress in indium (III) sulfide ($In_2S_3$) buffer layer deposition techniques for CIS, CIGS, and CdTe-based thin film solar cells, Solar Energy 120 (2015) 131–146.
3. N. Barreau, Indium sulfide and relatives in the world of photovoltaics, Solar Energy 83 (2009) 363–371.
4. R.Scheer and H.-W. Schock, Chalcogenide Photovoltaics, WILEY-VCH Verlag & Co. KGaA, 2011.
5. N. Naghavi, S. Spiering, M. Powalla, D. Lincot (2003) Record efficiencies for dry processed cadmium free CIGS solar cells with indium sulfide buffer layers prepared by atomic layer deposition (ALD). In: Proceedings of the 3rd World Conference on Photovoltaic Energy Conversion, vol. 1, Osaka, pp. 340–343.
6. R. Sáez-Araoz, J. Krammer, S. Harndt, T. Koehler, M. Krueger, P. Pistor, A. Jasenek, F. Hergert, M. Ch. Lux-Steiner, and C.-H. Fischer, ILGAR In2S3 buffer layers for Cd-free Cu(In, Ga)(S, $Se)_2$ solar cells with certified efficiencies above 16%. Prog. Photovolt.: Res. Appl. 20 (2012) 855–861.
7. C. Battaglia, A. Cuevasb and S. Wolf, High-efficiency crystalline silicon solar cells: status and perspectives, Energy Environ. Sci. 9 (2016) 1552.
8. N. P. Barradas, C. Jeynes, R.P. Webb, U. Kreissig, and R. Grötzschel, Rutherford backscattering analysis of thin films and superlattices with roughness, Nucl. Instrum. Methods Phys. Res. B149 (1999) 233.

9. A.S.Barrière, G.Couturier, A.Elfajri, G.Gevers, H.Guégan, B.Mombelli, and V.Tournay, Indium fluoride thin films prepared by sublimation under vacuum, Thin Solid Films 209 (1) (1992) 38–43.
10. N. Barreau, J.C. Bernedes, S. Marsillac, Study of the new β-In2S3 containing Na thin films. Part II: optical and electrical characterization of thin films, J. Cryst. Growth 241 (2002) 51–56.
11. R Swanepoel, Determination of the thickness and optical constants of amorphous silicon, J. Phys. E: Sci. Instrum. 16 (1983) 1214-1222.
12. S.H. Choe, T.H. Bang, N.O. Kim, H.G. Kim, C.I. Lee, M.S. Jin, S.K. Oh,W.T. Kim, Optical properties of β-In2S3 and β-In2S3:$Co_2$+ single crystals, Semicond. Sci. Technol. 16 (2001) 98.
13. R.S. Manea, C.D. Lokhande, Studies on structural, optical and electrical properties of indium sulfide thin films, Materials Chemistry and Physics 78 (2002) 15–17.
14. N. Naghavi, R. Henriquez, V. Laptev, and D. Lincot, Growth studies and characterisation of $In_2S_3$ thin films deposited by atomic layer deposition (ALD), Applied Surface Science 222 (2004) 65–73.
15. A. Timoumi, H. Bouzouita, M. Kanzari, and B. Rezig, Fabrication and characterization of $In_2S_3$ thin films deposited by thermal evaporation technique, Thin Solid Films 480–481 (2005) 124–128.
16. M.M. El-Nahass, B.A. Khalifa, H.S. Soliman, and M.A.M. Seyam, Crystal structure and optical absorption investigations on β-$In_2S_3$ thin films, Thin Solid Films 515 (2006) 1796–1801.
17. N. Barreau, J.C. Berne`de, S. Marsillac, C. Amory, W.N. Shafarman, New Cd-free buffer layer deposited by PVD: $In_2S_3$ containing Na compounds, Thin Solid Films 431–432 (2003) 326-329.
18. J. Schoneberg, M. Richter, J. Ohlanda, P. Eraerds, T. Dalibor b, J. Parisi, Electrical and optical analysis of $In_xS_y$:Na thin-films with varied sodium concentration as buffer layer in $Cu(In,Ga)(S,Se)_2$ solar cells, Thin Solid Films 633 (2017) 243–247.

## List of figure captions

**Figure 1**. RBS spectrum (a) and composition depth profile by two-layer model (b).

**Figure 2.** SEM micrograph of the ISF layer deposited on the silicon substrate.

**Figure 3**. Temperature dependence of the resistivity for the ISF film.

**Figure 4**. Transmittance spectrum of the ISF film.

**Figure 5.** Tauc's plots for direct (a) and indirect (b) interband optical transitions.

**Figure 6.** Spectral response of the ISF film.

Figures (if any)

Click here to download Figures (if any): Fig1ab.pdf

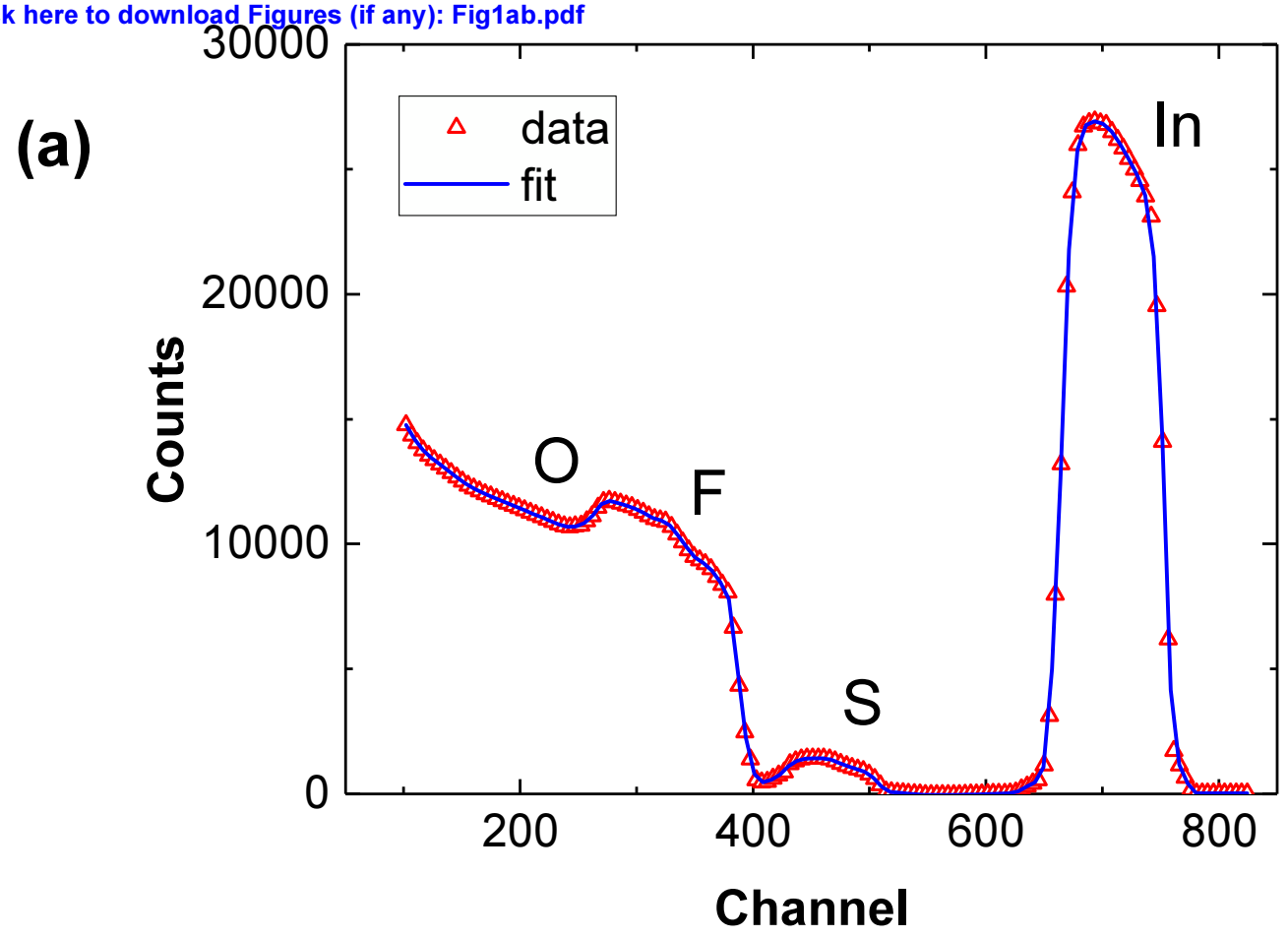


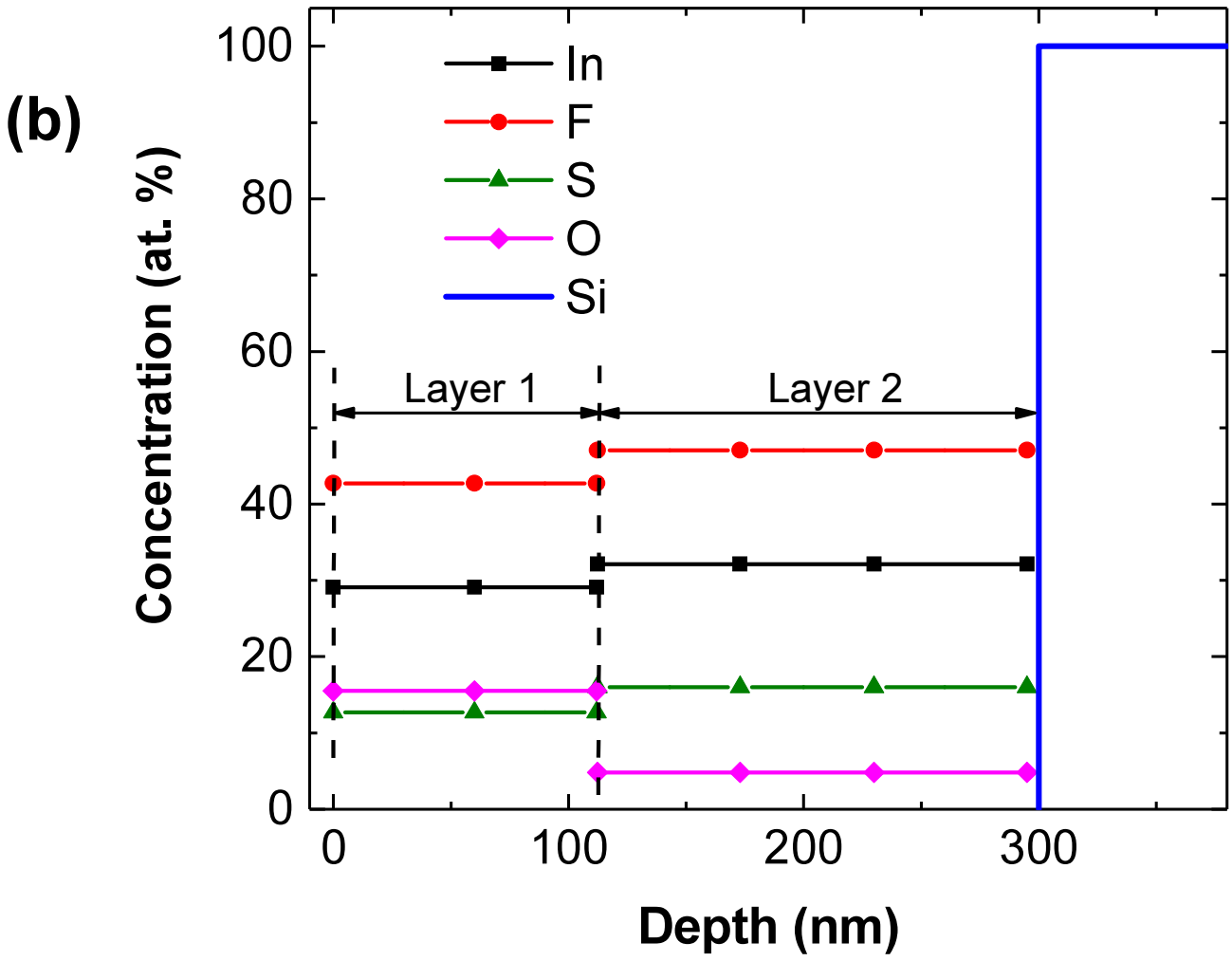

**Figures (if any)**
**Click here to download high resolution image**

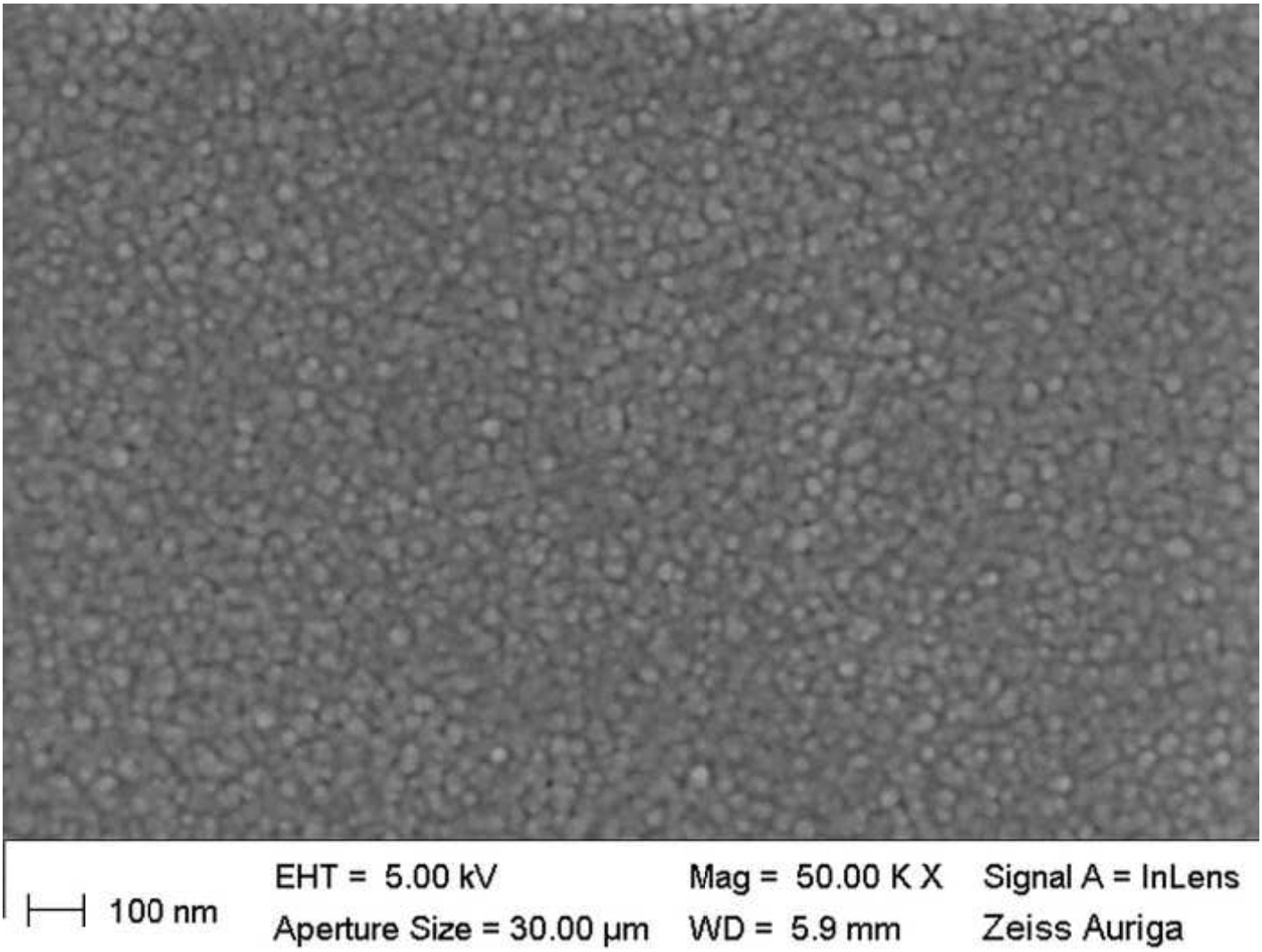

Figures (if any)
Click here to download Figures (if any): Fig_3.pdf

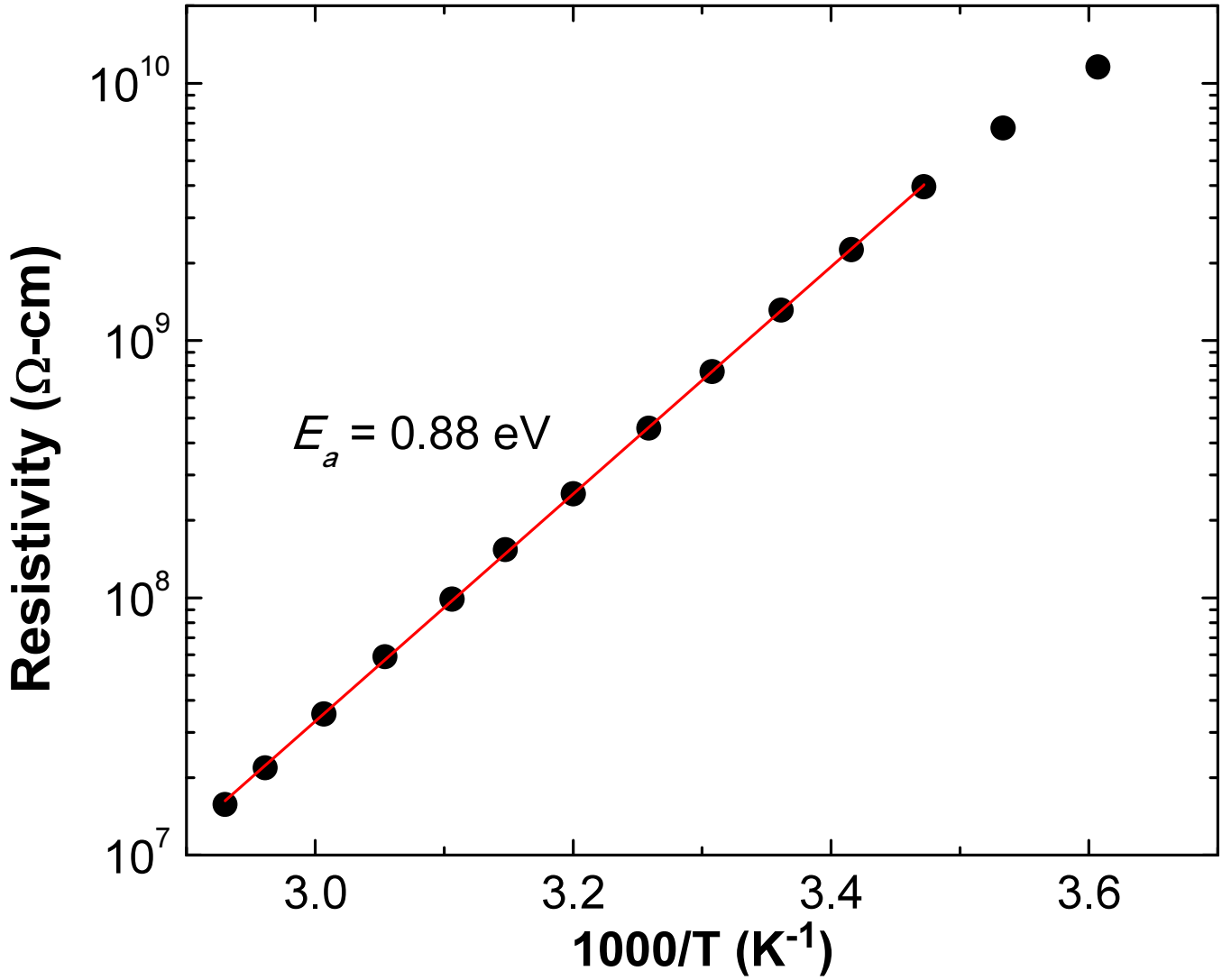

Figures (if any)
Click here to download Figures (if any): Fig_4.pdf

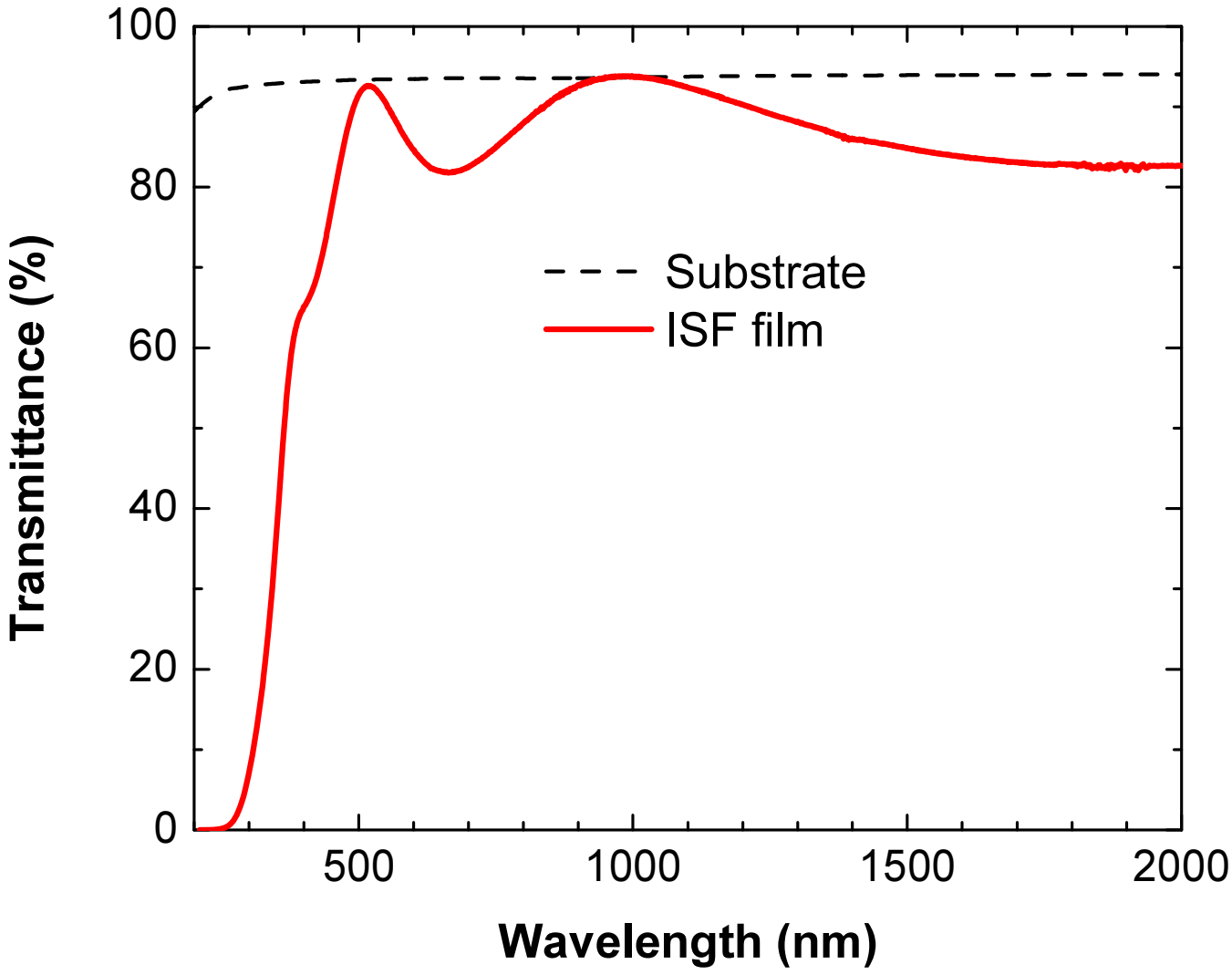

**Figures (if any)**
**Click here to download Figures (if any): Fig_5.pdf**

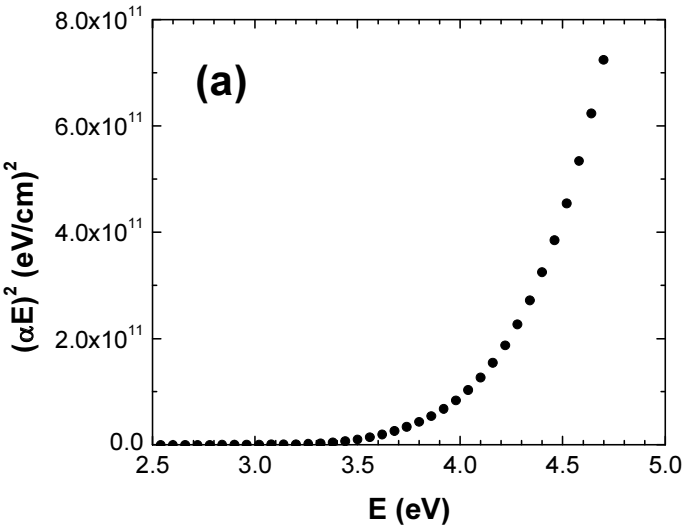


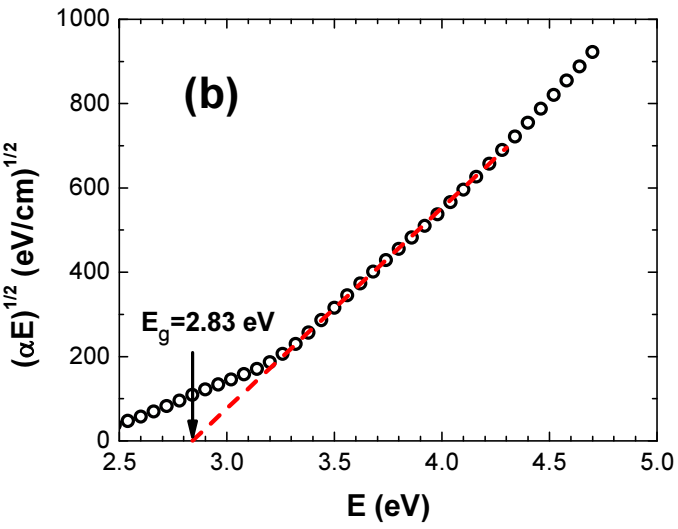

Figures (if any)
Click here to download Figures (if any): Fig_6.pdf